Investigation of the hydration properties of cement with EDTA by alternative current impedance spectroscopy

Chi, Lin; Li, Wenda ; Li, Zhenming; Wang, Zheng; Lu, Shuang ; Liu, Qi

DOI
10.1016/j.cemconcomp.2021.104365

Publication date
2022

Document Version
Final published version

Published in
Cement and Concrete Composites

Citation (APA)
Chi, L., Li, W., Li, Z., Wang, Z., Lu, S., & Liu, Q. (2022). Investigation of the hydration properties of cement with EDTA by alternative current impedance spectroscopy. *Cement and Concrete Composites*, *126*, 1-12. Article 104365. https://doi.org/10.1016/j.cemconcomp.2021.104365

Cement and Concrete Composites 126 (2022) 104365

Contents lists available at ScienceDirect

Cement and Concrete Composites

journal homepage: www.elsevier.com/locate/cemconcomp

Investigation of the hydration properties of cement with EDTA by alternative current impedance spectroscopy

Lin Chi [a,b], Wenda Li [b], Zhenming Li [c,*], Zheng Wang [b], Shuang Lu [b,**], Qi Liu [b]

[a] School of Environment and Architecture, University of Shanghai for Science and Technology, Shanghai, 200093, China
[b] School of Civil Engineering, Harbin Institute of Technology, Harbin, 150001, China
[c] Microlab, Faculty of Civil Engineering and Geoscience, Delft University of Technology, Delft, 2628, CN, the Netherlands

ARTICLE INFO

Keywords:
Cement hydration
Impedance
Microstructure
EDTA
Non-destructive testing

ABSTRACT

Alternative current impedance spectroscopy (ACIS) is a promising non-destructive testing method to monitor long-term change and assess the durability of concrete. This study investigates the influences of Ethylene Diamine Tetraacetic Acid (EDTA) on the hydration of hardening cement by ACIS. It is found that EDTA retards the early-age hydration of cement but can facilitate the later age reaction. Pastes with EDTA show comparable or higher compressive strength than Control at 28 d, especially when the dosage is higher than 0.4%. Microstructural characterization results reveal the working mechanism of EDTA originating from its complexing effect on free ions. The resistivity evolution of the pastes detected by ACIS can well reflect the effects of EDTA on the cement hydration in different ages. Proportional relations are identified between the resistivity and other hydration parameters, such as reaction degree, chemical shrinkage, compressive strength. The results of this study indicate a wider prospect of ACIS in monitoring the microstructure evolution and macro-properties of cementitious materials.

1. Introduction

Ordinary Portland cement (hereafter-termed cement) has been widely used for more than a century [1,2]. As a binder material, hardened cement shows good mechanical properties and durability. However, the hardened properties of cement paste and concrete are substantially determined by the hydration process and microstructure evolution during hardening or setting [3,4]. Therefore, enormous research attention has been attracted to the hardening process of cement. In the past decades, various methods have been utilized to characterize the hydration process of hardening cement, such as calorimetry, chemical shrinkage, ultrasonic velocity measurement, scanning electron microscope, etc. [5–8]. Besides, electrical methods to measure the resistance, impedance and other electrical parameters are proved feasible and convenient to monitor the hydration process of cement [9–11]. By applying current on the materials, the structure evolution of cement can be monitored by resistivity or impedance non-destructively.

In fact, alternative current (AC) impedance spectroscopy technique has been long used to study the properties of the electronic materials and element measurement, but the application of this method in cement or concrete started only in recent decades [12–14]. It is known that the hardening process of cement involves the percolation of the solid skeleton, reduction in free water and also changes in the concentrations of ions in the pore solution. All these effects would induce changes in the resistivity of the materials with time. Many studies have been conducted to measure the resistivity evolution of cement and found that the reliability of the direct current method is doubtful since the ions in the paste (mainly in the pore solution) will rearrange under direct current and cause electrode effect, thus influencing the obtained resistivity of cement [15]. In comparison, a big advantage of AC method with various frequencies is that the electrode effect can be avoided, therefore the measured impedance can intrinsically illustrate the property of cement paste [16].

From 1990s, Gu et al. started to use AC impedance spectroscopy (ACIS) in monitoring the hydration of cement and built equivalent circuit model for the paste [17]. AC impedance could indicate the capillary water content in concrete and thus could reflect the concrete quality [18]. It was identified by Gu et al. [19] that the angle and diameter of the semicircle in the Nyquist plot both closely relate to the pore size distribution of the paste, while the high frequency resistance of cement

* Corresponding author.
** Corresponding author.
E-mail addresses: z.li-2@tudelft.nl (Z. Li), lus@hit.edu.cn (S. Lu).

https://doi.org/10.1016/j.cemconcomp.2021.104365
Received 2 August 2021; Received in revised form 18 November 2021; Accepted 28 November 2021
Available online 1 December 2021

paste is mainly determined by the porosity of solid and the ions concentration in pore solution. In recent years, an increasing number of studies have been conducted on the application of ACIS in cementitious materials [20–23]. For example, Silva et al. investigated the parameters obtained from the equivalent impedance circuit to characterize the effect of nanomaterials in cement-based mortars [20]. Vipulanandan et al. used electrical resistivity to evaluate the cement behavior and determine the effects on piezoresistivity variation under different curing conditions [21]. Dong et al. [24] found that by measuring the electrical properties of the cementitious composites, carbonation behavior could be monitored. Hong et al. [25] and Wei et al. [10] applied the resistivity parameters to predict the standard compressive strength of cementitious materials. The influences of supplementary cementing materials (SCMs) such as silica fume, fly ash and blast furnace slag on the impedance of the paste were studied by the same authors Li et al. [26,27].

In summary, the current literatures on ACIS are mainly about building of equivalent circuit model and the correlations between cement hydration and electrical parameters. Although various cement types, water/cement ratios and SCMs were studied, very few studies have considered the influences of chemical admixtures on the AC impedance of cement paste. Unlike SCMs that mainly influence the composition of the hydration products, chemical admixtures can significantly modify the reaction kinetics of the paste [28]. In practice, different hardening rates of cement are required by different applications, therefore, admixtures that can adjust the hardening rate of cement paste or concrete, such as retarders and accelerators, are usually used. However, whether ACIS method is still applicable in monitoring the hardening process of these systems has not been understood.

The aim of this study, therefore, is to characterize the hydration process of cement with retarder by ACIS and to identify the correlations between the resistivity and other hydration parameters. EDTA as a commonly used retarder is added into the cement mixture with various dosages. The setting time, workability, reaction heat, chemical shrinkage, element concentrations in the pore solution, reaction products and compressive strength of the pastes are comprehensively measured. The working mechanisms of EDTA revealed by ACIS are also discussed.

2. Materials, mixtures and methods

2.1. Raw materials and chemical admixtures

Ordinary Portland cement 42.5 N/R CEM I (OPC) produced by Yatai Harbin Building Materials® is used in this study. The chemical composition of the cement is shown in Table 1. The water to mix with cement was tap water. For the analysis of element concentrations in the pore solution, in particular, deionized water was used to make the paste. EDTA-Na (powder, purity 99.0%) with the formula of $C_{10}H_{12}N_2Na_4O_8{\cdot}2H_2O$ was used as the retarder.

2.2. Mixtures

Cement paste mixtures with various dosages of admixtures were studied, as shown in Table 2. Despite, the water/cement ratio of all mixtures was kept constant to control the variables. The cement powder was mixed with admixtures first for 4 min before water was added. The mixture was mixed at a low speed for 2 min and then high speed for another 2 min.

Table 1
Chemical compositions of the cement.

Oxide (wt. %)	CaO	Al_2O_3	SiO_2	MgO	Fe_2O_3	SO_3	Na_2O
Cement	62.31	5.50	21.05	1.72	3.92	2.66	0.47

Table 2
Mixture proportions of the cement paste.

Mixtures*	Water/cement ratio	EDTA (wt. %)
Control	0.35	0
E0.2		0.2
E0.4		0.4
E0.6		0.6

*E denotes for EDTA.

2.3. Experimental methods

2.3.1. Framework

The framework of the experiments conducted in this study is shown in Fig. 1. The fresh and hardened properties of the pastes with and without EDTA are measured at first. The reaction kinetics of the mixtures is then detected. To further understand the influence of EDTA on the paste, the solid reaction products and element concentration in the pore solution are then characterized. Next, all the properties and parameters are correlated with the AC impedance of the mixtures to explore the feasibility of using AC impedance to reflect the hydration process of the paste with EDTA. The details of individual experimental methods are given in the following sections.

2.3.2. Setting time and flowability

The initial and final setting times of the paste were measured according to ASTM C191-19 [29]. The flowability of the paste was measured according to ASTM C1437-20 [30].

2.3.3. Compressive strength

Paste samples without electrodes embedded inside were cast in molds with the dimension of $20 \times 20 \times 20$ mm^3 for compressive strength test according to ASTM C 109/109M − 21 [31]. The samples were cured in standard curing room (relative humility >65%, temperature 21 ± 1 °C) after demoulding till the age of strength tests. The loading rate during the test was 2400 N/s ± 200 N/s.

2.3.4. Degree of hydration

The degree of hydration of the paste was estimated by the chemically bound water concrete based on Powers' model [32], as shown in Eq. (1).

$$\alpha=[(m_1\text{-}m_2) \times (m_2 \times \mathrm{LOI})\text{-}m_2 \times \mathrm{LOI}]/(0.23\ m_2) \quad (1)$$

where m_1 is the mass of cement paste after drying in the oven at 105 °C for 24 h until a constant mass is reached and m_2 is the mass of cement paste after igniting in the furnace at 1050 °C for 1 h. LOI represents the loss of ignition of the raw cement powder.

The value 0.23 was used based on the assumption that 0.23 g chemically bound water would be produced when 1 g of cement totally hydrates. The degree of hydration was thus calculated as the ratio between the chemically bound water content and 0.23 g per gram of cement.

2.3.5. Chemical shrinkage

The chemical shrinkage of cement paste mixtures was measured according to dilatometry. The detailed procedure was as specified in ASTM C 1608-17 Standard test method for chemical shrinkage of hydraulic cement paste [33].

2.3.6. Hydration heat

Calorimetry test was used to monitor the early-age hydration heat of the cement paste mixtures. The test last for 3 d at isothermal condition at 21 °C. The reaction heat results were normalized by the weight of cement.

2.3.7. Reaction products and element concentration

To further investigate the influences of EDTA on the hydration

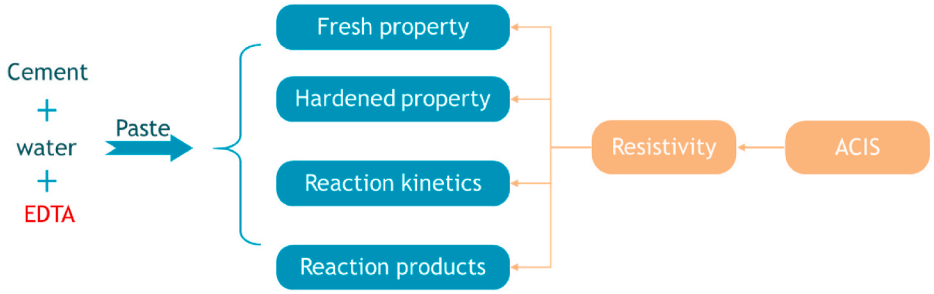

Fig. 1. Experimental framework of this study.

products of cement paste, X-ray diffraction (XRD) and Thermal gravimetric analysis (TGA) were utilized to test the solid part (ground into powder) and ICP spectrometer was used to test the liquid part (pore solution) of the paste, respectively.

The paste Control and E0.4 cured for 6 h, 12 h, 24 h and 28 d were ground into powder samples after hydration stoppage. XRD test was conducted using a X'Pert PRO MPD powder X-ray diffractometer, with Cu K_α radiation, tube setting to be 40 kV and 45 mA, a step size of 0.02°, and a 2 θ range of 10–70°. TGA was measured within Argon environment within a temperature range of 30 °C–900 °C. The temperature-increasing rate was 10 °C/min.

The concentrations of elements (Ca, Na, K and Si) in the pore solution of Control and E0.4 were measured. The pore solution of early-age paste was extracted by an Instron (SBT-PSE/D45) when the paste was cured for 3 h, 6 h, 12 h and 24 h.

2.3.8. AC impedance and resistivity

An apparatus was developed in this study to measure the AC impedance of cement paste. Stainless steel meshes with an effective conductive size of 45 mm × 25 mm was chosen for the electrode [34]. The electrodes were passivated and do not easily participate in cement hydration. Cement paste was cast in between the two meshes so that the

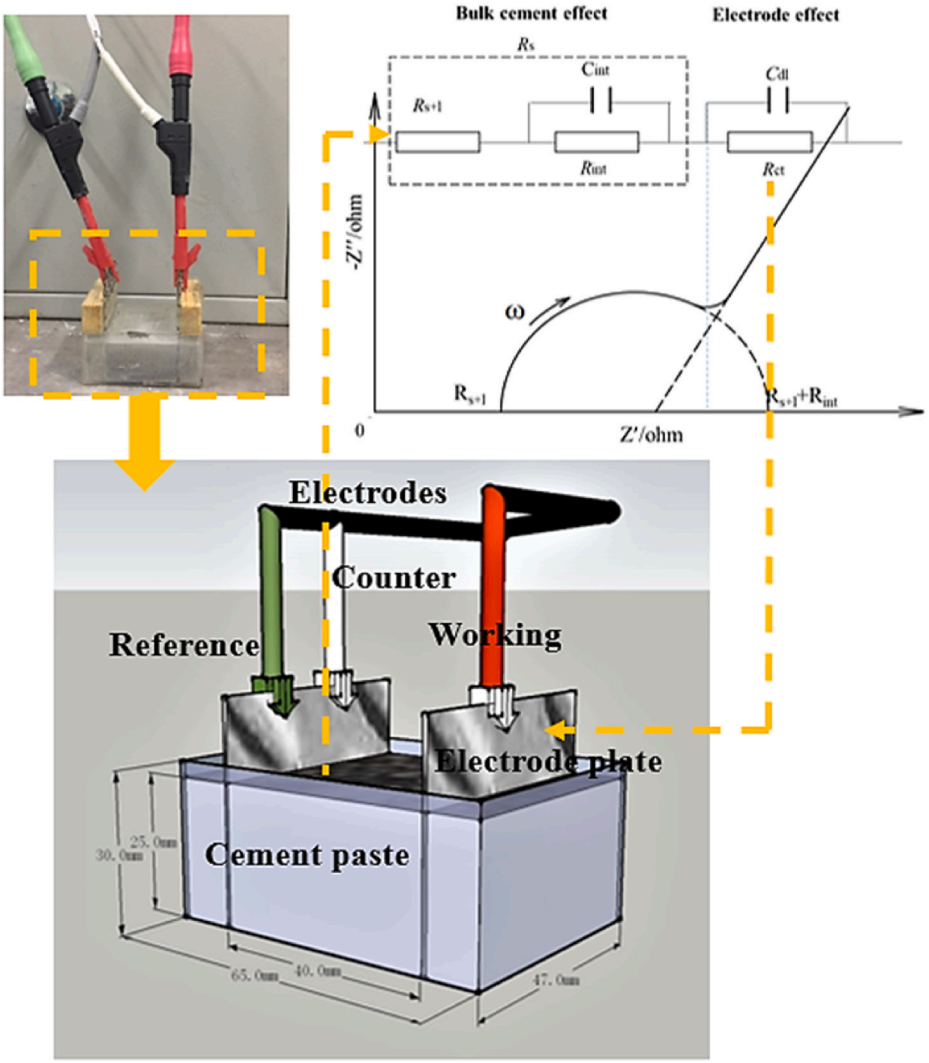

Fig. 2. Classic Nyquist model and equivalent circuit of the electrode-cement paste system.

metal was embedded into the paste, as shown in Fig. 2. The paste was sealed by plastic film to avoid moisture loss.

An electrochemical workstation (VersaSTAT 4000A, Ameteck Scientific Instruments Inc.) was used to measure the AC impedance of the sample under frequencies from 1Hz to 10 MHz. The amplitude of the sine-wave alternating current was 100 mV. To obtain sufficient information in the early age, the AC impedance was measured every 10 min in the first day after casting. Afterwards, the samples were immersed in the saturated lime water of the curing tank in the curing room with 21 °C. Before AC measurement, the surface moisture of samples was wiped off. The AC measurement was conducted every day and the test for each sample lasted for 2 min. Before the measurement, two null tests were conducted to eliminate the fluctuation of mold and wires. Each sample was tested five times to reduce fluctuations. After the test, samples were sent back to the curing room immediately. Resistivity is sensitive to moisture content and temperature, influencing the accuracy and reliability. Due to the small volume of the paste and the delayed exothermic heat of cement paste with EDTA, the temperature effect for cement paste at the early age is not apparent in our system.

The bulk resistance can be obtained from AC impedance measurement according to the equivalent circuit $R\{RC\}\{RC\}$ [19]. In this study, the bulk resistance is considered as the sum of the resistances of the liquid and solid ($R_{t(s+l)}$) and the liquid/solid interface ($R_{t(int)}$). $R_{t(s+l)}$ denotes the total resistance of solid and liquid phases; $R_{t(int)}$ and $C_{t(int)}$ denotes the resistance and capacitance of the solid-liquid interface, respectively; R_{ct} and C_{dl} denotes the resistance and capacitance of the paste-electrode interface, respectively [35]. The subscript t indicates that the resistance or capacitance of the paste changes with time.

To verify the accuracy of the apparatus, the resistance of standard KCl solutions with the concentrations of 0.1 mol/L and 1 mol/L was measured and compared with the theoretical value. The error was found to be within 2%, thus confirming that the facility is reliable. Detailed results of this part can be found in Appendix A.

3. Results and discussion

3.1. Properties of cement pastes with and without EDTA

3.1.1. Setting time and flowability

The setting time and flowability results of the paste with and without EDTA are shown in Fig. 3. It can be seen that the setting time of the paste increases when more EDTA is added into the mixture without exception. This indicates the role of EDTA as a retarder for fresh cement paste. When the dosage of EDTA is 0.8%, the paste does not set until 21 h. The spread of paste increases when EDTA is present, as shown in Fig. 3, revealing an improved flowability of the paste. This effect is more pronounced for dosages of 0.2% and 0.4%.

3.1.2. Compressive strength

Fig. 4 shows the compressive strength of the mixtures with different dosages of EDTA. The strength of all samples increases with curing age. The 1 d and 3 d-strength of the paste decreases with the incorporation of EDTA. No strength is shown when the content of EDTA reaches 0.8%. The strength of E0.4 exceeds that of Control from 7 d, while other mixtures are still weaker than Control. At 28 d, the mixtures with EDTA show comparable or higher compressive strength than Control. In general, EDTA has a strong effect to reduce the strength development of paste at the early age, especially when the dosage is higher than 0.4%. However, all mixtures show similar strength irrespective of the content of EDTA at 28 d. These results indicate that EDTA hinders the hydration of cement at the early age. This point will be verified in the next section.

3.1.3. Reaction kinetics

3.1.3.1. Degree of hydration. The degree of hydration of the pastes determined by chemically bound water content is shown in Fig. 5. It can be observed that the degree of reaction of paste with EDTA is lower than that of the control at the early age. The mixtures show similar reaction degrees to that of Control at 7 d. Afterwards the effect of EDTA is not pronounced. The reaction degrees of all the mixtures at 7 d are around 0.8 times of that at 28 d, indicating a major part of the reaction has been finished in the first 7 d.

It is also interesting to note that the evolution of the reaction degrees of various mixtures with time correspond well with that of the compressive strength (see Figs. 4 and 5). A mixture with higher reaction degree generally shows a higher compressive strength. This indicates that EDTA influences the strength of the paste mainly by influencing the reaction rate. According to the similar strength and degrees of reaction of the mixtures at 28 d, it seems EDTA would not result in defects in the paste in long term.

3.1.3.2. Reaction heat. The early-age heat flow and accumulative reaction heat of the pastes are shown in Fig. 6. Fig. 6 a) shows that the initial heat flow peaks of mixtures with EDTA are higher than that of Control. The initial heat peak is normally attributed to the dissolution of the cement [36]. The results in Fig. 6 a) indicate that EDTA can facilitate the dissolution of cement at the beginning of reaction (see the inserted panel). The dormant or induction period of the mixtures are longer when more EDTA is added. The main heat peak of E0.6 does not appear within 3 d. Meanwhile, the main heat peaks of mixture with EDTA are lower but

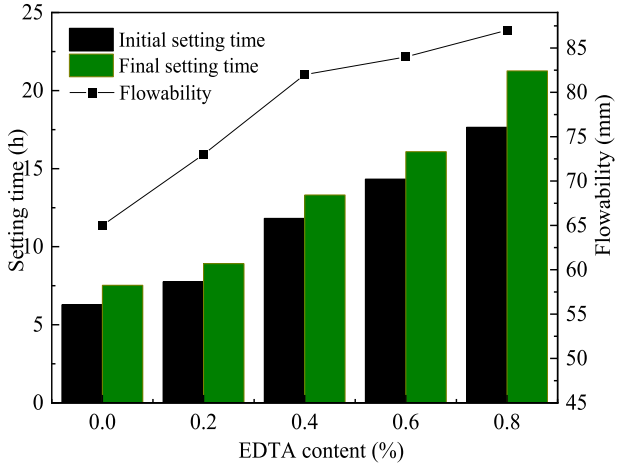

Fig. 3. Setting times and flowability of the pastes.

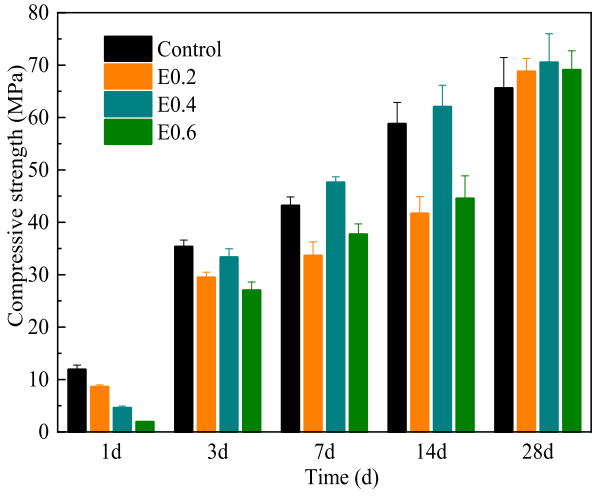

Fig. 4. Compressive strength of the pastes with various EDTA content.

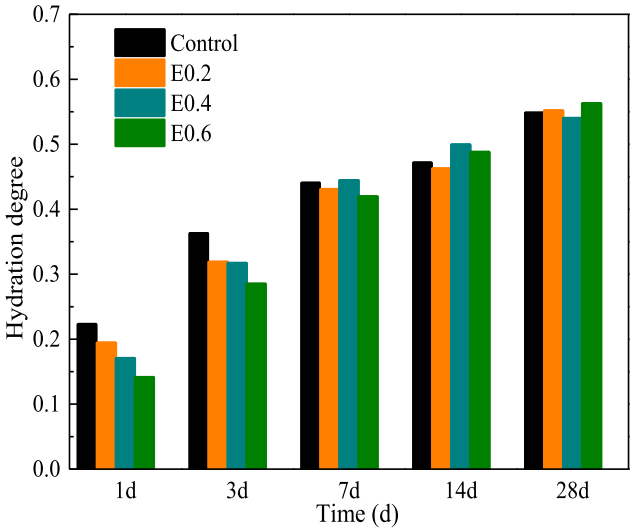

Fig. 5. Degree of hydration of the pastes.

wider. This might be due to that the ions dissolved from the cement particles are bound to EDTA, so that less ions participate in the reactions forming products until the deceleration period. This point will be verified in the following sections. Fig. 6 b) shows that the total reaction heat of Control, E0.2 and E0.4 is not much different, while the one of E0.6 is significantly lower than others, which is consistent with the lower 3d-strength of E0.6.

3.1.3.3. Chemical shrinkage. Chemical shrinkage is another parameter that can reflect the reaction kinetics of cement paste. In the first 4 h, the chemical shrinkages of the pastes are not readily distinguished, but afterwards, the chemical shrinkage of Control exceeds the others, as shown in Fig. 7 a). The more EDTA is present, the lower chemical shrinkage is shown at 1 d, which is consistent with the chemically bound water and calorimetry results (Figs. 5 and 6). It is also noted that the moments when the second surges of chemical shrinkage of the mixtures occur also correspond with the starting time of the acceleration period measured by calorimetry. At 28 d, the chemical shrinkages of EDTA mixtures are comparable or even higher than that of Control, which coincides with the compressive strength results shown in Fig. 4.

3.1.4. Reaction products and pore solution

The reaction products and pore solution of E0.4 cured for different ages are characterized and compared with that of Control to further understand the influence of EDTA on the hydration process.

3.1.4.1. TGA results. It can be seen in Fig. 8 that the first endothermic peaks of both Control and E0.4 are at around 100 °C when the samples are less than 1 d. These peaks are due to the loss of water from the sample. At 28 d, by contrast, these peaks fall in around 150 °C since more water is physically or chemically bound in the paste thus needs higher temperature to be evaporated.

The second endothermic peak at around 450 °C is due to the decomposition of portlandite (CH). $CaCO_3$ typically decompose at from 600 °C to 750 °C [37]. Based on the mass loss in corresponding temperature ranges, the amounts of CH and $CaCO_3$ produced in the pastes can be quantified, as presented in Fig. 8e) and f).

It can be seen from Fig. 8 f) that the presence of 0.4% of EDTA hinders the formation of CH in cement paste at the early age. This is probably due to the absorption of Ca^{2+} by EDTA as discussed above. With the increase of curing age, the CH contents in both Control and E0.4 increase. At 28 d, the CH content in E0.4 is a bit higher than in Control, as consistent with the slightly higher strength and hydration degree of E0.4 shown above. The content of $CaCO_3$ shows similar trends in the two mixtures.

The similar DTA-TG curves of the two mixtures at 28 d (Fig. 8 d)) and

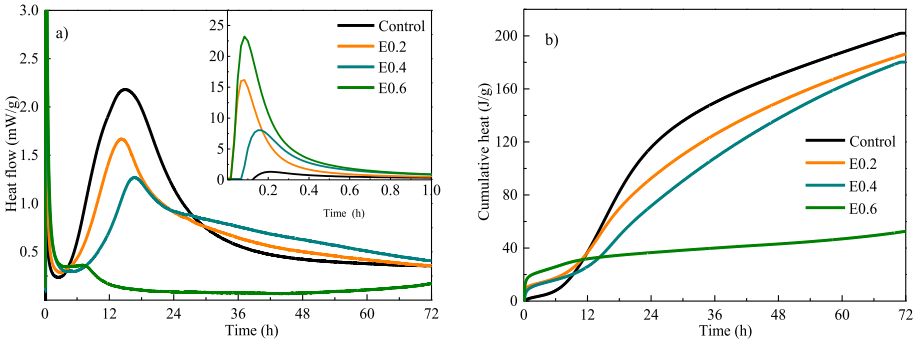

Fig. 6. Heat flow a) and accumulative heat b) of the pastes in the first 3 d.

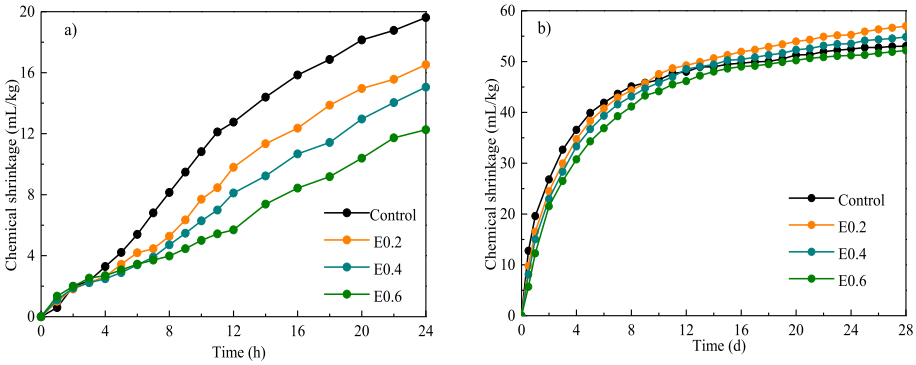

Fig. 7. Chemical shrinkage of the pastes in 24 h a) and 28 d b).

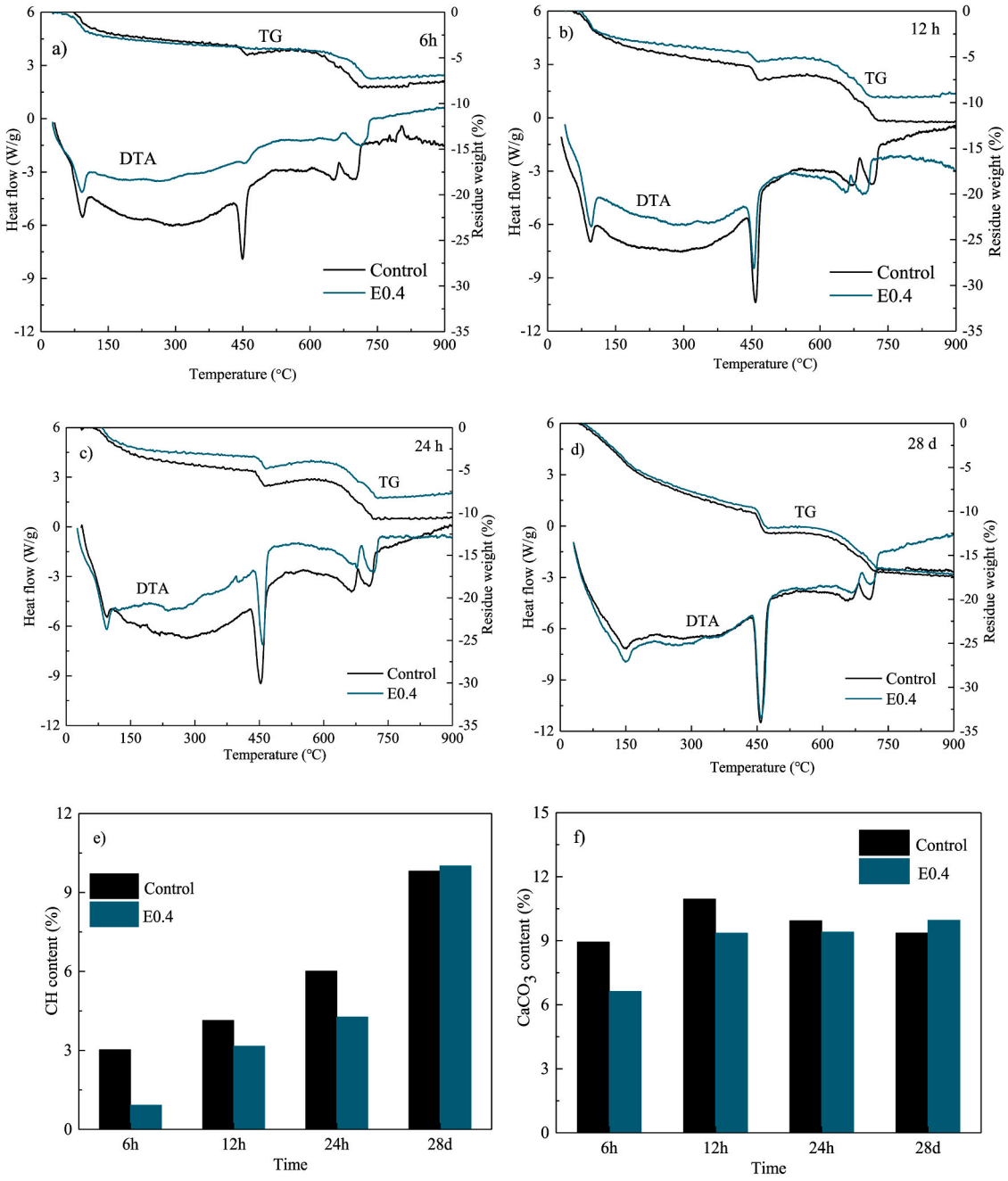

Fig. 8. DTA-TG curves of E0.4 cured for 6 h a), 12 h b), 24 h c) and 28 d d) and the quantified CH e) and $CaCO_3$ f) contents.

the similar contents of crystals in this age (Fig. 8 e)-f)) indicate that EDTA has limited influences on products formation in long term.

3.1.4.2. XRD results. The lower amounts of CH and $CaCO_3$ in E0.4 in the first day determined by TGA find evidence in XRD results. It can be seen in Fig. 9 that the bands of CH and $CaCO_3$ in the diffraction spectrum of E0.4 are lower than in spectrum for Control. Besides, the intensity of C_3S band is apparently higher for E0.4 than for Control within the first day, indicating that EDTA hinders the hydration of C_3S. At 28 d, the spectra of the two mixtures are basically the same.

3.1.4.3. Element concentration. In general, the presence of EDTA leads to higher concentrations of K^+, Na^+ and Ca^{2+}, as shown in Fig. 10. As shown in Section 3.1.3, EDTA facilitates the dissolution of cement. This is probably because EDTA as a complexant can absorb metals ions and form complexes, resulting in higher element concentrations, but lower ions concentrations in the pore solution. In return, the dissolution of cement particles is enhanced to compensate the loss of cations in the pore solution. This point is verified in this section. Once bound to EDTA, the metal complexes are less likely to form precipitates in short period.

Among the metals, Ca^{2+} is the most important element for the formation of hydrates and is therefore gradually consumed. This is the reason why a general decreasing concentration of Ca^{2+} is observed for both Control and E0.4, while the concentrations of K^+ and Na^+ both increase with curing age. Similar evolution to Ca^{2+} is observed for Si^{4+}, which is another ingredient of C–S–H. At 24 h, very small amounts of Ca^{2+} and Si^{4+} exist in the pore solution of both Control and E0.4.

The improved workability, reduced early-age hydration rate and comparable 28 d strength indicate that EDTA is a promising retarder to be used in cement paste. It would be interesting if ACIS can reflect the

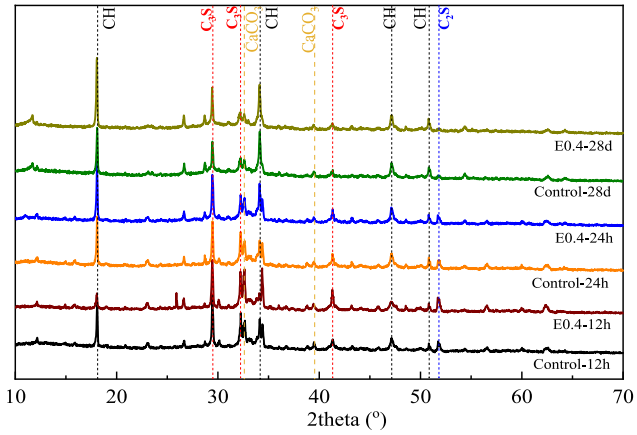

Fig. 9. XRD spectra for Control and E0.4 cured for 12 h, 24 h and 28d.

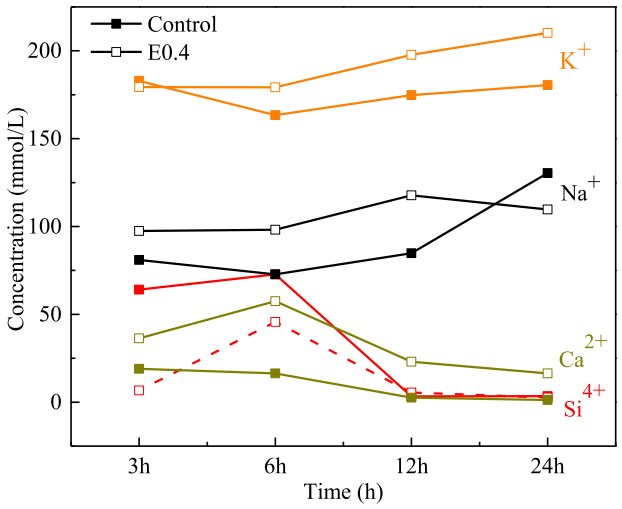

Fig. 10. Concentrations of K^+, Na^+, Ca^{2+} and Si^{4+} in pore solutions of Control and E0.4 during first 24 h.

hydration parameters of cement paste with EDTA. The working mechanism of EDTA will be further elaborated with the help of ACIS results shown in the next section.

3.2. AC impedance and resistivity

3.2.1. AC impedance

To obtain the impedance of the cement paste under alternative current, equivalent circuit needs to be built at first. In this paper, the equivalent circuit $R\{RC\}\{RC\}$ is chosen due to its high accuracy in simulating the responds of cement paste, as shown in Fig. 2 [19]. The paste is considered as a porous insulator base with electrolyte in the pores and the solid, liquid and interface are considered as serial in the circuit.

An example of the Nyquist plot, i.e. the one for Control and E0.4 at different curing ages is plotted in Fig. 11. The impedance data was normalized with respect to surface area of the stainless steel meshes. Real part of the electrical impedance Z_{rel}, which is the sum of $R_{t(s+l)}$ and $R_{t(int)}$, can be obtained directly by experiments.

The software ZSimpWin3.5 (EChem Software) was used to obtain the parameters from equivalent circuit, such as $R_{t(s+l)}$, $R_{t(int)}$, R_{ct}, C_{int}, C_{dl} and n_1 and n_2. Detailed discussion on the methodology has been elaborated in our previous studies [34,35]. Herein, only the resistivity of the mixtures with and without EDTA are listed while other parameters are put in Appendix B.

3.2.2. Evolution of resistivity with curing age

The resistivity results of the pastes with and without EDTA at different ages are shown in Fig. 12. Several reaction stages can be clearly distinguished in the curves. As shown in Fig. 12 (a), the resistivity of Control decreases at first before increases after 1 h. The decrease is due to the dissolution of cement particles which releases ions, e.g., K^+, Na^+, Ca^{2+}, SiO_4^{4-}, and OH^-, into the water or initial pore solution. The resistivity slightly increases afterwards and more or less stabilizes. This does not mean the stoppage of the dissolution but an equilibrium in ions between dissolution and early-age precipitation. This period corresponds to the induction period as shown in Fig. 6. When EDTA is present, the turning point of the curve prior to the acceleration period is delayed due to the enhanced dissolution of the paste.

From 5 to 7 h, the mixtures experience a second decrease in resistivity. This small decrease can be attributed to the second surge of dissolution of cement when the cover of cement particles formed by initial products breaks. This argument can be verified by the intense increase of concentrations of K^+ and Na^+ from 6 h to 12 h, as shown in Fig. 10. It is noted that the hydration already falls into acceleration period according to the heat release results as shown in Fig. 6. The second surge of dissolution probably contributes to the heat release in the start of this period. Other explanations of the second decrease in resistivity are proposed by different researchers [38–40]. For example, El-Enein et al. proposed that the slight decrease in resistivity in this stage is caused by the formation of AFm ($C_3A{\cdot}CaSO_4{\cdot}18H_2O$) from AFt ($C_3A{\cdot}3CaSO_4{\cdot}32H_2O$), which releases extra Ca^{2+} and SO_4^{2-} [39]. Therefore, this mechanism seems also plausible.

From 9 to 12 h, depending on the mixture, the resistivity of the pastes increases sharply, as shown in Fig. 12 (a). This is because the percolation of the paste when a lot of hydration products form and the connectivity of pores reduces. As shown in Fig. 10, the concentrations of ions do not severely drop from 12 h to 24 h. Therefore, the increase of resistivity is due to the less transport paths of ions rather than less ions. With the incorporation of EDTA, the increase comes later which is consistent with the retarded formation of hydration products as discussed above.

From 4 to 6 d, the increasing rate of the resistivity slows down indicating the formation of a stable mixture with dense microstructure and low reaction rate. The resistivity evolves in the same pace as the chemical shrinkage shown in Fig. 7. The resistivity of paste is lower for mixture with more EDTA. This indicates that EDTA improved the connectivity of the pores in cement-matrix. Fig. 4 shows that the 28d strength of the mixtures are similar. However, compressive strength is mainly dependent on the porosity, while the electrical resistivity reflects also the pore connectivity [41]. When EDTA is present, the cement particles are better dispersed, and less agglomeration would occur, so that the pores are also more evenly distributed and connected in the paste, which ensures more paths for the ions transport. From this point of view, the resistivity can also be used as an indicator of the pore connectivity of the pastes.

3.2.3. Relations between resistivity and other parameters

Quantitative relations can be identified between the resistivity and other hydration parameters.

Fig. 13 a) shows a strong linear relation between the compressive strength and electrical resistivity of cement pastes. This indicates that the ACIS is more suitable to reflect the hardening process of cement when the ions concentrations experience dramatic changes. In the long term, the connectivity of the pores plays the main role in influencing the resistivity [42,43]. EDTA can improve the 28 d-strength by a more homogenous microstructure but would reduce the resistivity of the paste since the pores are more connected.

Exponential relations are also observed between resistivity (ρ) and other hydration parameters such as degree of hydration (α) and

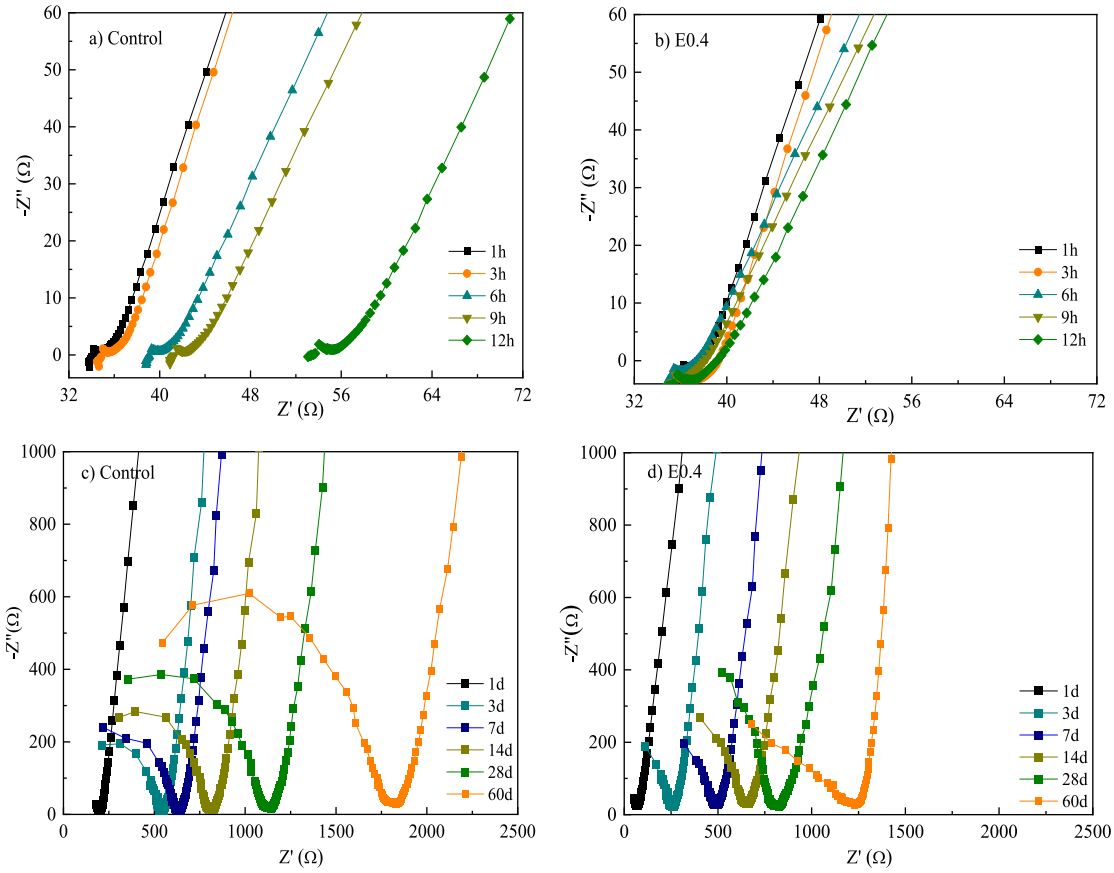

Fig. 11. Nyquist plots of Control and E0.4 at 1–12 h a) b) and 1–60 c) d).

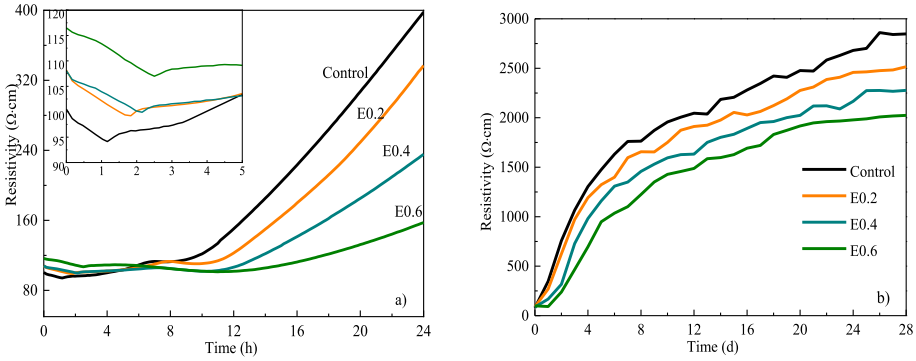

Fig. 12. Resistivity of the pastes at the curing age of 1–24 h a) and 1–28 d b).

cumulative hydration heat of the pastes, as shown in Fig. 13b) and c). The correlation coefficient between the degree of hydration and electrical resistivity at the early age of 1–3 d is much higher than that of the age of 3–28 d in Fig. 13 b), which can be verified by the correlation between resistivity and cumulative heat of hydration at 1–3 d in Fig. 13 c). The resistivity of the pastes is also plotted together with the chemical shrinkage in Fig. 13 d). The slopes of the curves for EDTA-containing mixtures are very close to each other, indicating that the dosage of EDTA does not lay intrinsically impact on the microstructure development of cement paste. With the known resistivity, the chemical shrinkage of an EDTA mixture can be roughly predicted. However, the resistivity of EDTA mixtures is lower than that of Control at a given chemical shrinkage when it exceeds 40 g/ml. This may be due to that the pores in EDTA-containing paste are more evenly distributed due to the dispersing effect of EDTA on cement particles during mixing. With the same chemical shrinkage, the free water contents in the pastes would be similar [44], but EDTA-containing mixtures have better transport networks of water and ions, thus their resistivity is lower than Control.

The results in Fig. 13 indicate that the resistivity results can be used to estimate the hydration degree of the paste with various contents of EDTA. According to Powers' model, the degree of hydration α can be calculated with Eq. (2) [45,46]. A correlation of chemical shrinkage, isothermal calorimetry test, chemical bound water of cement paste with various EDTA content can be conducted and extended as Eq. (3).

$$\alpha = \frac{W_n(t)}{W_n^0} = \frac{Q(t)}{Q^0} = \frac{CS(t)}{CS^0} \tag{2}$$

$$\alpha = \frac{W_n(t)}{W_n^0} = \frac{Q(t)}{Q^0} = \frac{CS(t)}{CS^0} = D\frac{\mathrm{Ln}(k_1\rho_t)}{\mathrm{Ln}(k_2\rho_{\mathrm{total}})} \tag{3}$$

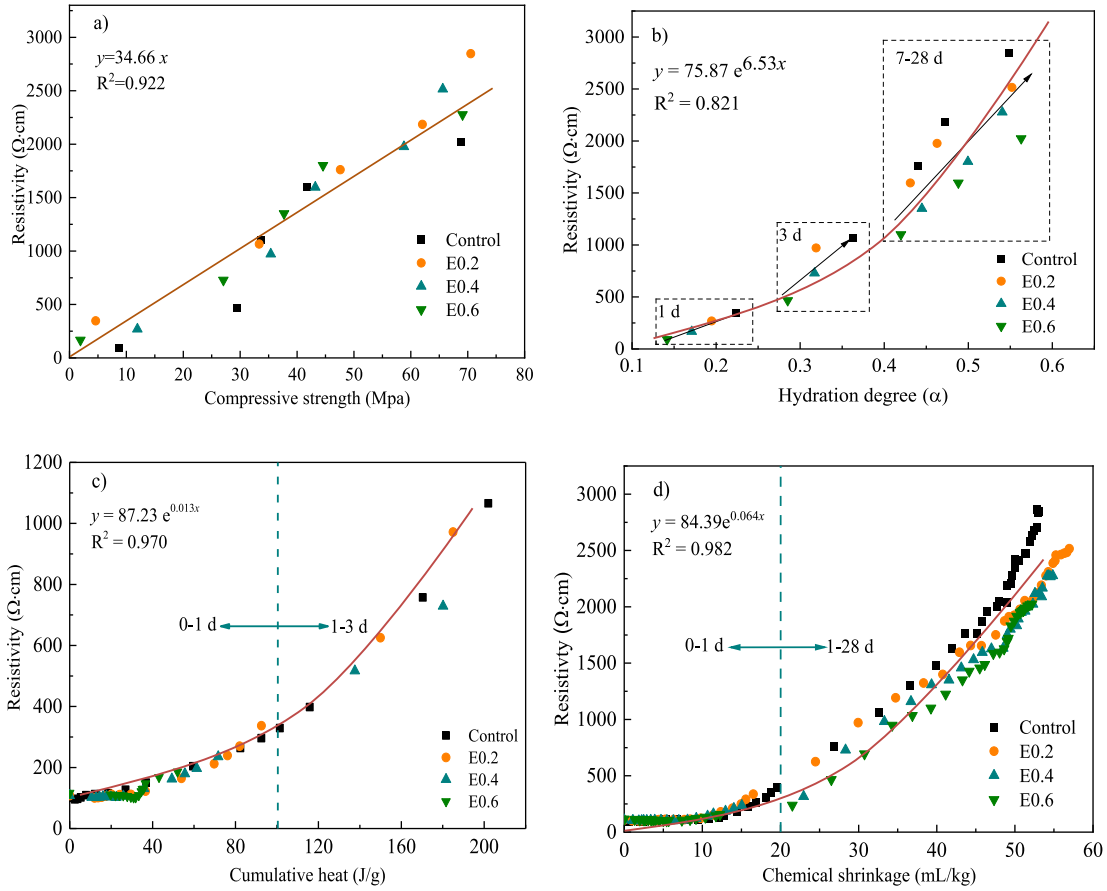

Fig. 13. Relations between resistivity and compressive strength a), degree of hydration b) cumulative heat c) and chemical shrinkage d) of the pastes.

where $W_n(t)$ and W^0 are chemically bond water content at time t and at fully hydration, in g/g cement; $Q(t)$ and Q^0 are cumulative heat evolution at time t and at fully hydration, in J/g cement; and $CS(t)$ and CS^0 are the chemical shrinkage at time t and at fully hydration, in mL/g; ρ(t) and ρ_{total} are electrical resistivity at time t and at fully hydration, in Ω·cm; k_1, k_2 and D are fitting parameters related to the cement composites.

There are mathematical correlations expressed between electrical resistivity and the hydration parameters such as degree of hydration, chemical shrinkage, cumulative heat release and compressive strength. Considering majority of the hydration parameters cannot be monitored continuously, by collecting the electrochemical parameters of the hydration process of cement-based materials, the mechanical strength and hydration process can be nondestructively monitored, and a health monitoring system can be established to provide theoretical basis for the intelligent monitoring of the structure in the future.

3.3. Discussion

Based on the microstructure characterization and new indications generated from AC impedance analysis, we can see that the evolution of AC resistivity of paste with time can precisely reflect the hydration processes of cement paste with and without EDTA, especially at the very early age. The poor crystallized hydrates at the early-age correspond to the EIS responses in Nyquist curves for hydrating cements. The magnitude of the resistivity at late age can indicate the influence of EDTA on the pore structure of the paste. Positive or even linear relationships exist between the resistivity and other hydrating parameters of the paste, such as setting time, hydration degree and 1d compressive strength. Through various techniques, especially ACIS, the working mechanism of EDTA in cement paste is clarified, as shown in Fig. 14.

The mechanism behind is hypothesized as the binding capacity of EDTA [46]. When EDTA is added into cement paste, EDTA molecules are easy to be absorbed onto the surface of cement particles and the function groups (e.g. -COO^-) of EDTA can bind cations such as Ca^{2+}, Mg^{2+} and Fe^{3+}. The reduced concentrations of free ions in the pore solution, in return, enhance the initial dissolution of cement particles to compensate the ions loss. As a result, the heat flow of pastes with EDTA is higher than that of Control at the beginning of the mixing (Fig. 6). The concentration of ions is lower when EDTA is present, while that of element is not (Fig. 10). The absorption of EDTA together with the bounded ions onto the cement particles provides a larger repulsive force between particles, resulting in a better dispersed suspension and thus a better workability of the paste (Fig. 3 (b)). The connection and bonding between cement particles are more difficult to build due to the repulsive force [48,49], which contributes to a later setting of the paste (Fig. 3 (a)). The binding by EDTA leads to lower concentrations of free ions, e.g., Ca^{2+}, which would participate into the reactions forming products, which is known as the chelation competition process. Thus, longer dormant periods and lower reaction degrees (Fig. (5)-(9)) are shown by the pastes with EDTA. Consequently, the 1 d strength of these mixture is also lower (Fig. 4). However, the absorbed layer of EDTA and the complexes formed are not stable [50]. The ions would be released to the pore solution and precipitate, and eventually reached a dynamic equilibrium [51]. Therefore, the 28 d-strength and reaction degree of the paste are rarely influenced by EDTA (Figs. 4 and 5).

4. Conclusions

In this study, the effects of EDTA on cement paste are investigated. ACIS is used to characterize the hydration process of pastes. Correlations

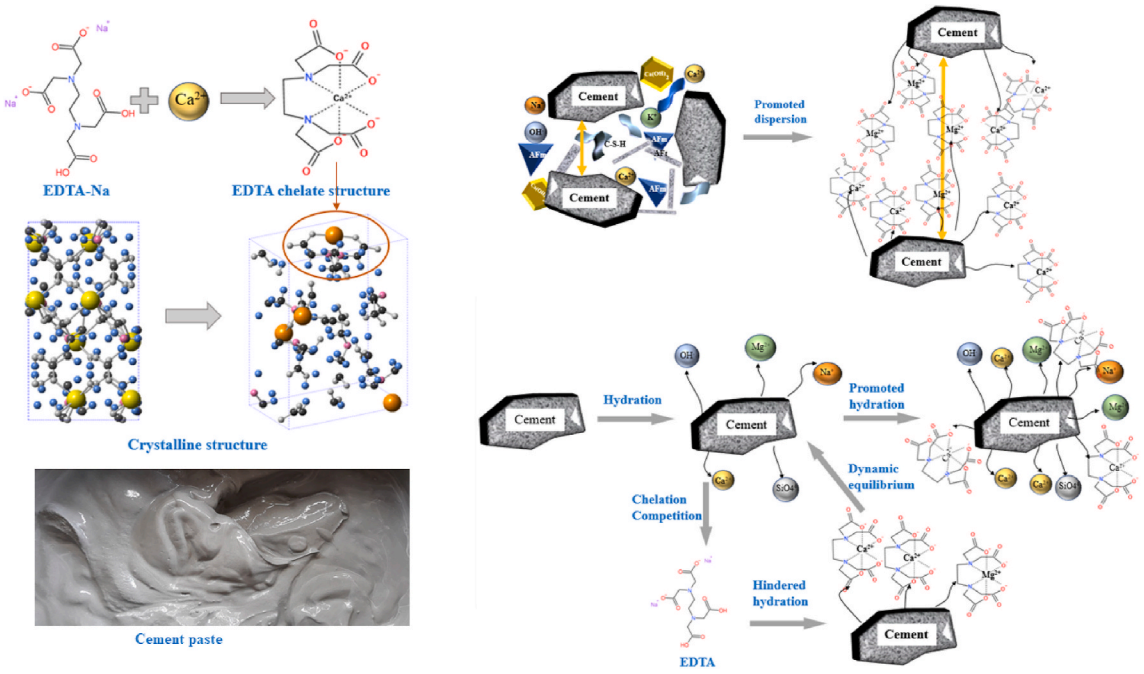

Fig. 14. Mechanism of EDTA on the hydration of cement paste.

between the AC resistivity and the hydration parameters are identified. The main conclusions of this study are listed below:

1. The dispersion of cement in the suspension is improved and a better workability of the paste with EDTA is achieved. Pastes with EDTA show comparable or higher compressive strength than Control at 28 d, especially when the dosage is higher than 0.4%.
2. Considering the free ions bounded by EDTA hindering the precipitation of hydration products, the reaction degree, chemical shrinkage and 1d strength are lower for EDTA-containing pastes. However, the complexes formed by EDTA are not stable and eventually reached a dynamic equilibrium. The 28d strength of the paste is rarely influenced by EDTA.
3. The evolution of resistivity obtained through ACIS precisely characterize the multiple hydration stages of cement pastes irrespective of the dosage of EDTA. Besides, proportional relations are identified between the resistivity and other hydration parameters, such as setting time, compressive strength, chemical shrinkage, cumulative heat and hydration degree.
4. The results in this study suggest that EDTA is an effective retarder for cement paste and ACIS is a promising non-destructive technique to reveal the reaction mechanisms and predict the hydration parameters of cementitious materials.

CRediT authorship contribution statement

Lin Chi: Conceptualization, Methodology, Funding acquisition. Wenda Li: Data curation, Formal analysis, Investigation. Zhenming Li: Writing- Original Draft, Writing- Reviewing and Editing. Zheng Wang: Validation. Shuang Lu: Supervision, Funding acquisition. Qi Liu: Visualization.

Declaration of competing interest

The authors declare that they have no known competing financial interests or personal relationships that could have appeared to influence the work reported in this paper.

Acknowledgment

The authors would like to appreciate the financial sponsored by Shanghai Sailing Program No.20YF1431800 and National Natural Science Foundation of China No.51872064.

Appendix

Appendix A

The measured resistivity of KCl solutions with concentrations of 0.1 mol/L and 1 mol/L are shown in Table A.1. The error between the measured results and the theoretical values, 85.893 Ω cm and 10.028 Ω cm, are also shown in the tables.

Table A.1
Resistivity of cell filled with 0.1 mol/L and 1 mol/L KCl solution (Ω·cm)

	Concentration KCL (0.1 mol/L)	Concentration KCL (0.01 mol/L)
1st	87.159	11.017
2nd	87.418	11.075
3rd	87.649	11.046
Average	87.409	11.046
Error	1.8%	0.1%

Appendix B

All electrical parameters obtained from Nyquist plots of mixtures with and without EDTA are shown inTable B.1-B.4 .

Table B.1
Detailed parameters of circuit fitting in Nyquist curves of Control in Fig. 11 a)

Age (h)	$R_{t(s+"}$>+l) (Ω·cm)	R_{ct} (Ω·cm)	C_{dl} (pF·cm^{-1})	n_2
1	34.76	4.33E+13	180.5	0.885
3	35.25	9.48E+11	177.5	0.888
6	39.96	1.36E+13	189.5	0.850
9	42.19	1.70E+10	191.7	0.842
12	55.08	5.66E+12	190.3	0.840
24	104.5	4.64E+14	184.9	0.832

Table B.2
Detailed parameters of circuit fitting in Nyquist curves of E0.4 in Fig. 11 b)

Age (h)	$R_{t(s+"}$>+l) (Ω·cm)	R_{ct} (Ω·cm)	C_{dl} (pF·cm^{-1})	n_2
1	36.10	3.62E+10	171.1	0.813
3	36.96	1.42E+11	167.7	0.824
6	37.12	2.76E+10	175.3	0.816
9	38.02	1.89E+12	182.4	0.815
12	38.44	7.89E+12	188.0	0.814
24	83.78	3.13E+13	191.3	0.816

Table B.3
Detailed parameters of circuit fitting in Nyquist curves of Control in Fig. 11 c)

Age (d)	$R_{t(s+"}$>+l) (Ω·cm)	$R_{t(int)}$ (Ω·cm)	R_{ct} (Ω·cm)	C_{int} (nF·cm^{-1})	n_1	C_{dl} (pF·cm^{-1})	n_2
3	47.26	477.8	5.79E+11	0.431	0.871	186.1	0.868
7	96.10	526.0	7.92E+12	0.489	0.868	196.8	0.866
14	82.39	709.3	1.16E+14	0.422	0.862	194.5	0.864
28	105.12	980.1	1.01E+13	0.416	0.850	189.1	0.849
60	165.33	1590	2.65E+13	0.514	0.826	197.2	0.769

Table B.4
Detailed parameters of circuit fitting in Nyquist curves of E0.4 in Fig. 11 d)

Age (d)	$R_{t(s+"}$>+l) (Ω·cm)	$R_{t(int)}$ (Ω·cm)	R_{ct} (Ω·cm)	C_{int} (nF·cm^{-1})	n_1	C_{dl} (pF·cm^{-1})	n_2
3	53.78	205.35	4.84E+14	0.431	0.804	155.7	0.813
7	86.43	393.69	3.59E+13	0.485	0.816	176.8	0.862
14	100.44	540.17	9.74E+14	0.473	0.785	171.3	0.815
28	96.81	712.84	7.98E+14	0.470	0.828	169.7	0.819
60	143.72	1081.95	1.44E+15	0.442	0.837	184.9	0.812

References

[1] W. Zhang, X. Yao, T. Yang, Z. Zhang, The degradation mechanisms of alkali-activated fly ash/slag blend cements exposed to sulphuric acid, Construct. Build. Mater. 186 (2018) 1177–1187.

[2] C. Shi, A.F. Jiménez, A. Palomo, New cements for the 21st century: the pursuit of an alternative to Portland cement, Cement Concr. Res. 41 (2011) 750–763.

[3] J. Liu, J. Li, J. Ye, F. He, Setting behavior, mechanical property and biocompatibility of anti-washout wollastonite/calcium phosphate composite cement, Ceram. Int. 42 (2016) 13670–13681.

[4] P. Mácová, A. Viani, Investigation of setting reaction in magnesium potassium phosphate ceramics with time resolved infrared spectroscopy, Mater. Lett. 205 (2017) 62–66.

[5] A.J.N. MacLeod, F.G. Collins, W. Duan, Effects of carbon nanotubes on the early-age hydration kinetics of Portland cement using isothermal calorimetry, Cement Concr. Compos. 119 (2021) 103994, 10.

[6] Z. Li, S. Zhang, Y. Zuo, W. Chen, G. Ye, Chemical deformation of metakaolin based geopolymer, Cement Concr. Res. 120 (2019) 108–118.

[7] S. Czarnecki, M. Shariq, M. Nikoo, A. Sadowski, An intelligent model for the prediction of the compressive strength of cementitious composites with ground granulated blast furnace slag based on ultrasonic pulse velocity measurements, Measure 172 (2021) 108951.

[8] M. Harihanandh, K.E. Viswanathan, A.R. Krishnaraja, Comparative study on chemical and morphology properties of nano fly ash in concrete, Mater. Today: Proce. 45 (2021) 3132–3136.

[9] H. Wang, A. Zhang, F. Shi, J. Liu, P. Cao, T. Du, H. Gu, Development of relationships between permeability coefficient and electrical and thermal conductivity of recycled aggregates permeable cement concrete, Construct. Build. Mater. 254 (2020) 119247.

[10] X. Wei, L. Xiao, Z. Li, Prediction of standard compressive strength of cement by the electrical resistivity measurement, Construct. Build. Mater. 31 (2012) 341–346.10.

[11] S.W. Tang, X.H. Cai, Z. He, W. Zhou, H.Y. Shao, Z.J. Li, T. Wu, E. Chen, The review of early hydration of cement-based materials by electrical methods, Construct. Build. Mater. 146 (2017) 15–29.

[12] X. Hu, C. Shi, X. Liu, J. Zhang, G. de Schutter, A review on microstructural characterization of cement-based materials by AC impedance spectroscopy, Cement Concr. Compos. 100 (2019) 1–14.
[13] Y. Zhu, H. Zhang, Z. Zhang, Y. Yao, Electrochemical impedance spectroscopy (EIS) of hydration process and drying shrinkage for cement paste with W/C of 0.25 affected by high range water reducer, Construct. Build. Mater. 131 (2017) 536–541.
[14] F.S.G. Aldo, L.P. John, Electrochemical cell design and impedance spectroscopy of cement hydration, J. Mater. Sci. 56 (2021) 1–18.
[15] Y. Zuo, J. Zi, X. Wei, Hydration of cement with retarder characterized via electrical resistivity measurements and computer simulation, Construct. Build. Mater. 53 (2014) 411–418.
[16] I. Shakir Abbood, S.S. Weli, F.L. Hamid, Cement-based materials for self-sensing and structural damage advance warning alert by electrical resistivity, Mater. Today: Proce. 46 (2021) 615–620.
[17] P. Gu, P. Xie, J.J. Beaudoin, R. Brousseau, A.C. impedance spectroscopy (I): a new equivalent circuit model for hydrated portland cement paste, Cement Concr. Res. 22 (1992) 833–840.
[18] W.J. Mccarter, T.M. Chrisp, G. Starrs, J. Blewett, Characterization and monitoring of cement-based systems using intrinsic electrical property measurements, Cement Concr. Res. 33 (2003) 197–206.
[19] P. Gu, P. Xie, J.J. Beaudoin, Application of A.C. impedance techniques in studies of porous cementitious materials : (I): influence of solid phase and pore solution on high frequency resistance, Cement Concr. Res. 23 (1993) 531–540.
[20] G.F. Da Silva, S. Martini, J.C.B. Moraes, L.K. Teles, AC impedance spectroscopy (AC-IS) analysis to characterize the effect of nanomaterials in cement-based mortars, Construct. Build. Mater. 269 (2021) 121260.
[21] C. Vipulanandan, K. Ali, Smart Portland cement curing, piezoresistive behaviour with montmorillonite clay soil contamination, Cement Concr. Compos. 91 (2018) 42–52, 10.1016.
[22] F. Yousuf, X. Wei, J. Tao, Evaluation of the influence of a superplasticizer on the hydration of varying composition cements by the electrical resistivity measurement method, Construct. Build. Mater. 144 (2017) 25–34.
[23] F. He, R. Wang, C. Shi, C. Chen, L. Lin, X. An, Error evaluation and correction of stray impedance during measurement and interpretation of AC impedance of cement-based materials, Cement Concr. Compos. 72 (2016) 190–200.
[24] B. Dong, Q. Qiu, Z. Gu, J. Xiang, C. Huang, Y. Fang, F. Xing, W. Liu, Characterization of carbonation behavior of fly ash blended cement materials by the electrochemical impedance spectroscopy method, Cement Concr. Compos. 65 (2016) 118–127.
[25] S. Hong, J. Zhang, H. Liang, J. Xiao, C. Huang, G. Wang, H. Hu, Y. Liu, Y. Xu, F. Xing, B. Dong, Investigation on early hydration features of magnesium potassium phosphate cementitious material with the electrodeless resistivity method, Cement Concr. Compos. 90 (2018) 235–240.
[26] H. Pei, H. Shao, Z. Li, A novel early-age shrinkage measurement method based on non-contact electrical resistivity and FBG sensing techniques, Construct. Build. Mater. 156 (2017) 1158–1162.
[27] B. Chen, H. Shao, B. Li, Z. Li, Influence of silane on hydration characteristics and mechanical properties of cement paste, Cement Concr. Compos. 113 (2020) 103743.
[28] Y. Wang, C. Shi, Y. Ma, Y. Xiao, Y. Liu, Accelerators for shotcrete-Chemical composition and their effects on hydration, microstructure and properties of cement-based materials, Construct. Build. Mater. 281 (2021) 122557.
[29] ASTM C191-19, Standard Test Methods for Time of Setting of Hydraulic Cement by Vicat Needle, ASTM International, West Conshohocken, PA, 2019. www.astm.org.
[30] ASTM C1437-20, Standard Test Method for Flow of Hydraulic Cement Mortar, ASTM International, West Conshohocken, PA, 2020. www.astm.org.
[31] ASTM C109/C109M-21, Standard Test Method for Compressive Strength of Hydraulic Cement Mortars (Using 2-in. Or [50 Mm] Cube Specimens), ASTM International, West Conshohocken, PA, 2021.
[32] E.I. Nadelman, K.E. Kurtis, Application of Powers' model to modern portland and portland limestone cement pastes, J. Am. Ceram. Soc. 100 (2017) 4219–4231.
[33] ASTM C1608-17, Standard Test Method for Chemical Shrinkage of Hydraulic Cement Paste, ASTM International, West Conshohocken, PA, 2017. www.astm.org.
[34] L. Chi, Z. Wang, S. Lu, H. Wang, K. Liu, W. Liu, Early assessment of hydration and microstructure evolution of belite-calcium sulfoaluminate cement pastes by electrical impedance spectroscopy, Electrochim. Acta 389 (2021) 138699.
[35] L. Chi, Z. Wang, S. Lu, D. Zhao, Y. Yao, Development of mathematical models for predicting the compressive strength and hydration process using the EIS impedance of cementitious materials, Construct. Build. Mater. 208 (2019) 659–668.
[36] Y. Sargam, K. Wang, Hydration kinetics and activation energy of cement pastes containing various nanoparticles, Compos. B Eng. 216 (2021) 108836.
[37] L. Qin, X. Gao, T. Chen, Influence of mineral admixtures on carbonation curing of cement paste, Construct. Build. Mater. 212 (2019) 653–662.
[38] A. Arabzadeh, M.A. Notani, A. Kazemiyan Zadeh, A. Nahvi, A. Sassani, H. Ceylan, Electrically conductive asphalt concrete: an alternative for automating the winter maintenance operations of transportation infrastructure, Compos. B Eng. 173 (2019) 106985.
[39] R. Palod, S.V. Deo, G.D. Ramtekkar, Effect on mechanical performance, early age shrinkage and electrical resistivity of ternary blended concrete containing blast furnace slag and steel slag, Mater. Today: Proceedings 32 (2020) 917–922.
[40] C.E.T. Balestra, A.Y. Nakano, G. Savaris, R.A. Medeiros-Junior, Reinforcement corrosion risk of marine concrete structures evaluated through electrical resistivity: proposal of parameters based on field structures, Ocean. Eng. 187 (2019) 106167.
[41] K. Bharadwaj, R.M. Ghantous, F. Sahan, O.B. Isgor, W.J. Weiss, Predicting pore volume, compressive strength, pore connectivity, and formation factor in cementitious pastes containing fly ash, Cement Concr. Compos. 122 (2021) 104113.
[42] S.A. El-Enein, M.F. Kotkata, G.B. Hanna, M. Saad, M.M. AbdEl Razek, Electrical conductivity of concrete containing silica fume, Cem. Con. Res. 25 (1995).
[43] W. Li, X. Li, S.J. Chen, Y.M. Liu, W.H. Duan, S.P. Shah, Effects of graphene oxide on early-age hydration and electrical resistivity of Portland cement paste, Construct. Build. Mater. 136 (2017) 506–514.
[44] Z. Li, T. Lu, X. Liang, H. Dong, G. Ye, Mechanisms of autogenous shrinkage of alkali-activated slag and fly ash pastes, Cement Concr. Res. 135 (2020) 106107.
[45] X.Y. Pang, C. Meiyer, Cement chemical shrinkage as measure of hydration kinetics and its relationship with nonevaporable water, ACI Mater. J. 109 (2012).
[46] X. Pang, D.P. Bentz, C. Meyer, G.P. Funkhouser, R. Darbe, A comparison study of Portland cement hydration kinetics as measured by chemical shrinkage and isothermal calorimetry, Cement Concr. Compos. 39 (2013) 23–32.
[48] B. Yin, T. Kang, J. Kang, Y. Chen, L. Wu, M. Du, Investigation of the hydration kinetics and microstructure formation mechanism of fresh fly ash cemented filling materials based on hydration heat and volume resistivity characteristics, Appl. Clay Sci. 166 (2018) 146–158.
[49] Q. Liu, Z. Chen, Y. Yang, Model of the charged mosaic surface of the cement particle based on the adsorption behavior of surfactants using ATR-FTIR spectroscopy, Compos. B Eng. 215 (2021) 108802.
[50] N.A. DiBlasi, A.G. Tasi, X. Gaona, D. Fellhauer, K. Dardenne, J. Rothe, D.T. Reed, A. E. Hixon, M. Altmaier, Impact of Ca(II) on the aqueous speciation, redox behavior, and environmental mobility of Pu(IV) in the presence of EDTA, Sci. Total Environ. 783 (2021) 146993.
[51] K. Zhang, Z. Dai, W. Zhang, Q. Gao, Y. Dai, F. Xia, X. Zhang, EDTA-based adsorbents for the removal of metal ions in wastewater, Coord. Chem. Rev. 434 (2021) 213809.